

A SIMPLE MODEL FOR THE ABSORPTION OF STARLIGHT BY DUST IN GALAXIES

STÉPHANE CHARLOT¹

Institut d'Astrophysique de Paris, CNRS, 98 bis Boulevard Arago, 75014 Paris, France; charlot@iap.fr

AND

S. MICHAEL FALL

Space Telescope Science Institute, 3700 San Martin Drive, Baltimore, MD 21218; fall@stsci.edu

Received 1999 July 29 ; accepted 2000 February 28

ABSTRACT

We present a new model to compute the effects of dust on the integrated spectral properties of galaxies, based on an idealized prescription of the main features of the interstellar medium (ISM). The model includes the ionization of HII regions in the interiors of the dense clouds in which stars form and the influence of the finite lifetime of these clouds on the absorption of radiation. We compute the production of emission lines and the absorption of continuum radiation in the HII regions and the subsequent transfer of line and continuum radiation in the surrounding HI regions and the ambient ISM. This enables us to interpret simultaneously all the observations of a homogeneous sample of nearby ultraviolet-selected starburst galaxies, including the ratio of far-infrared to ultraviolet luminosities, the ratio of H α to H β luminosities, the H α equivalent width, and the ultraviolet spectral slope. We show that the finite lifetime of stellar birth clouds is a key ingredient to resolve an apparent discrepancy between the attenuation of line and continuum photons in starburst galaxies. In addition, we find that an effective absorption curve proportional to $\lambda^{-0.7}$ reproduces the observed relation between the ratio of far-infrared to ultraviolet luminosities and the ultraviolet spectral slope. We interpret this relation most simply as a sequence in the overall dust content of the galaxies. The shallow wavelength dependence of the effective absorption curve is compatible with the steepness of known extinction curves if the dust has a patchy distribution. In particular, we find that a random distribution of discrete clouds with optical depths similar to those in the Milky Way provides a consistent interpretation of all the observations. A noteworthy outcome of our detailed analysis is that the observed mean relations for starburst galaxies can be closely approximated by the following simple recipe: use an effective absorption curve proportional to $\lambda^{-0.7}$ to attenuate the line and continuum radiation from each stellar generation, and lower the normalization of the curve typically by a factor of 3 after 10^7 yr to account for the dispersal of the birth clouds. This recipe or our full model for absorption can be incorporated easily into any population synthesis model.

Subject headings: galaxies: ISM — galaxies: starburst — infrared: galaxies — ISM: dust, extinction — ultraviolet: galaxies

1. INTRODUCTION

To interpret the observed spectral properties of galaxies, we require models for both the production of stellar radiation and its transfer through the interstellar medium (ISM). Currently, the accuracy of population synthesis models contrasts with the rudimentary way in which the absorption of starlight by dust is often treated. In many applications, dust is either ignored or assumed to be distributed in a uniform screen in front of the stars. The resulting uncertainties in the absorption of the ultraviolet radiation in galaxies can be as much as an order of magnitude. This problem has become especially acute in studies of galaxies at high redshifts. Nearby starburst galaxies may be suitable analogs of high-redshift galaxies and provide important clues to interpreting their spectral properties. The observations of nearby ultraviolet-selected starburst galaxies are numerous, including the ratio of far-infrared to ultraviolet luminosities, the ratio of H α to H β luminosities, the H α equivalent width, and the ultraviolet spectral slope. In particular, there is a remarkably tight correlation between far-infrared luminosity and ultraviolet spectral slope (Meurer et al. 1995; Meurer, Heckman, & Calzetti 1999). This wealth of observations can po-

tentially help us quantify the effects of dust on various spectral properties of galaxies.

There have been several analyses of the spatial distribution and optical properties of the dust in nearby starburst galaxies based on various subsets of the observations (e.g., Fanelli, O'Connell, & Thuan 1988; Calzetti, Kinney, & Storchi-Bergmann 1994, 1996; Puxley & Brand 1994; Meurer et al. 1995; Gordon, Calzetti, & Witt 1997). A generic result of these studies is that if the dust is distributed in a uniform foreground screen, it must have an unusually grey extinction curve. Otherwise, the distribution must be patchy. However, these analyses also raise questions of how to account self-consistently for all the observations. For example, the absorption inferred from the H α /H β ratio in starburst galaxies is typically twice as high as that inferred from the ultraviolet spectral slope. One interpretation of this result is that the ionized gas and ultraviolet-bright stars have different spatial distributions (Calzetti 1997). Issues such as this highlight the need for a simple yet versatile model to interpret simultaneously a wide range of phenomena related to the absorption of starlight by dust in galaxies. The purpose of this paper is to present such a model.

¹Also Max-Planck Institut für Astrophysik, Karl-Schwarzschild-Strasse 1, 85748 Garching, Germany

We begin with the conventional view that young stars ionize HII regions in the interiors of the dense clouds in which they are born. Line photons produced in the HII regions and the non-ionizing continuum photons from young stars are absorbed in the same way by dust in the outer HI envelopes of the birth clouds and the ambient ISM. The birth clouds, however, have finite lifetimes. Thus, non-ionizing ultraviolet and optical photons from stars that live longer than the birth clouds are absorbed only by the ambient ISM. This allows the ultraviolet continuum to be less attenuated than the emission lines. Our model builds on several previous studies. For example, Silva et al. (1998) considered the effects of finite lifetimes of stellar birth clouds on the continuum but not the line emission from galaxies. Here, we treat the transfer of radiation (especially scattering) in an approximate way, which would preclude a detailed description of surface brightnesses but should be appropriate for angle-averaged quantities such as luminosities. Our model succeeds in accounting quantitatively for all the available observations of a homogeneous sample of nearby starburst galaxies.

We present our model in §2, where we express the effective absorption curve describing the global transmission of radiation in terms of the different components of the ISM. In §3, we compare our model with observations and identify the specific influence of each parameter on the different integrated spectral properties of galaxies. One outcome of our detailed analysis is a remarkably simple recipe for absorption, which provides a good approximation to the observed mean relations and is easy to incorporate into any population synthesis model. In §4, we explore how the spatial distribution of dust can be constrained by the observations. Our conclusions are summarized in §5.

2. DEFINITION OF THE MODEL

We first introduce some notation and nomenclature that will help specify our model. The luminosity per unit wavelength $L_\lambda(t)$ emerging at the time t from a galaxy illuminated by an internal stellar population can be expressed generally as

$$L_\lambda(t) = \int_0^t dt' \psi(t-t') S_\lambda(t') T_\lambda(t, t'). \quad (1)$$

Here $\psi(t-t')$ is the star formation rate at the time $t-t'$, $S_\lambda(t')$ is the luminosity emitted per unit wavelength and per unit mass by a stellar generation of age t' , and $T_\lambda(t, t')$ is the “transmission function,” defined as the fraction of the radiation produced at the wavelength λ at the time t by a generation of stars of age t' that escapes from the galaxy. Thus, $T_\lambda(t, t')$ must be regarded as the average transmission along rays emanating in all directions from all stars of age t' within the galaxy. Since absorption and scattering by dust will cause the radiation to emerge anisotropically to some degree, L_λ can only be measured by a hypothetical set of detectors completely surrounding the galaxy. In practice, this means that equation (1) gives the mean of $4\pi D^2 f_\lambda$, where D is the distance and f_λ is the observed flux, for an ensemble of randomly oriented but otherwise similar galaxies.

For some purposes, it is convenient to reexpress $L_\lambda(t)$ as the product of a mean transmission function weighted

by the luminosity of each stellar generation $\overline{T}_\lambda(t)$ and the total unattenuated stellar luminosity:

$$L_\lambda(t) = \overline{T}_\lambda(t) \int_0^t dt' \psi(t-t') S_\lambda(t'), \quad (2)$$

$$\overline{T}_\lambda(t) \equiv \frac{\int_0^t dt' \psi(t-t') S_\lambda(t') T_\lambda(t, t')}{\int_0^t dt' \psi(t-t') S_\lambda(t')}. \quad (3)$$

We often reexpress $\overline{T}_\lambda(t)$ in terms of an “effective absorption” optical depth $\hat{\tau}_\lambda(t)$ indicated by a caret and defined by

$$\overline{T}_\lambda(t) \equiv \exp[-\hat{\tau}_\lambda(t)]. \quad (4)$$

This nomenclature emphasizes that the luminosity of a galaxy is diminished purely by the absorption of photons.² However, since scattering may also affect the path lengths of the photons through the ISM before they are absorbed, $\hat{\tau}_\lambda(t)$ will differ in general from the true absorption curve determined by the optical properties of the dust grains. The fraction of stellar radiation not transmitted by the ISM, $1 - \overline{T}_\lambda(t)$, is absorbed by dust. Using equation (2) and integrating over all wavelengths, we obtain the total luminosity absorbed and reradiated by dust

$$L_{\text{dust}}(t) = \int_0^\infty d\lambda [1 - \overline{T}_\lambda(t)] \int_0^t dt' \psi(t-t') S_\lambda(t'). \quad (5)$$

We now specify our model for computing the above properties of galaxies. This amounts to specifying the transmission function $T_\lambda(t, t')$. Our goal is to parameterize only those features of the ISM that are essential to understanding the main physical effects of dust on the integrated spectral properties of galaxies. We adopt the simple but fairly conventional view illustrated in Figure 1. Young stars ionize HII regions in the inner parts of the dense (mostly molecular) clouds in which they are born. Line photons produced in the HII regions and the non-ionizing continuum photons from young stars propagate through the outer HI envelopes of these “birth clouds” and then through the “ambient ISM” before they escape from the galaxy. Both the HII and HI regions of the birth clouds may contain dust, and in the ambient ISM, the dust may be distributed in a smooth or patchy way. The birth clouds, however, have finite lifetimes. Thus, photons emitted by longer-lived stars propagate only through the ambient ISM—where they are treated in the same way as photons emerging from the birth clouds—before they escape from the galaxy. To incorporate these basic features into our model, we make the following simplifying assumptions.

We assume that stars form in clusters with the galaxy-wide stellar initial mass function (IMF). This should be an excellent approximation for the purpose of computing the integrated spectral properties of a galaxy, although it could break down in clusters or regions with small numbers of stars. In our model, all star clusters are embedded in their birth clouds for some time and then disrupt them or migrate away from them into the ambient ISM of the galaxy. We assume for simplicity that the effective absorption in the birth clouds depends only on the stellar age t'

²The optical depth $\hat{\tau}_\lambda$ defined by equation (4) has also been referred to by several other names in the literature, including the optical depth of “apparent extinction,” “effective extinction,” “attenuation,” “obscuration,” and “absorption.”

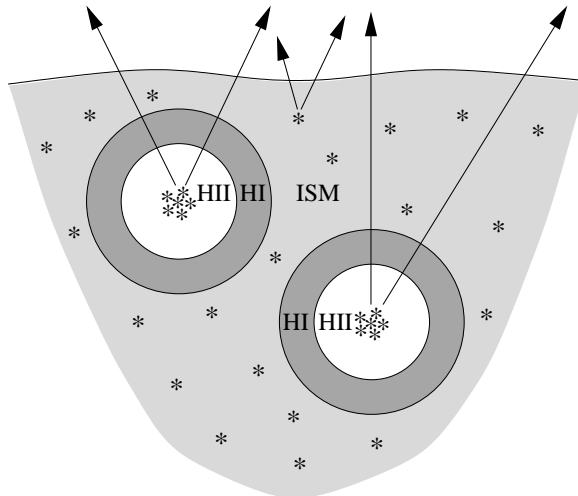


FIG. 1.— Schematic representation of the birth cloud and ambient ISM surrounding each generation of stars in a model galaxy (see text). Rays leaving in different directions are also shown.

and is constant in the ambient ISM. Hence, we can write the total transmission function in the form

$$T_{\lambda}(t, t') = T_{\lambda}^{\text{BC}}(t') T_{\lambda}^{\text{ISM}}, \quad (6)$$

where T_{λ}^{BC} and T_{λ}^{ISM} are the transmission functions of the birth clouds and the ambient ISM, respectively. In our model, the birth clouds, assumed to be identical, consist of an inner HII region ionized by young stars and bounded by an outer HI region. For simplicity, we assume that all stars remain within their birth clouds with a constant transmission function for a time t_{BC} and are then introduced immediately into the ambient ISM; thus

$$T_{\lambda}^{\text{BC}}(t') = \begin{cases} T_{\lambda}^{\text{HII}} T_{\lambda}^{\text{HI}}, & \text{for } t' \leq t_{\text{BC}}, \\ 1, & \text{for } t' > t_{\text{BC}}, \end{cases} \quad (7)$$

where T_{λ}^{HII} and T_{λ}^{HI} are the transmission functions of the HII and HI regions, respectively. By writing the transmission functions as products in equations (6) and (7), we have assumed that the propagation of photons in the HII and HI regions and the ambient ISM are independent of each other. This prescription is exact for forward scattering and should be a good approximation for the purpose of computing luminosities even with some backward scattering.

An alternative but equivalent way of expressing the transmission functions of the HII and HI regions and the ambient ISM is in terms of the corresponding effective absorption optical depths, $\hat{\tau}_{\lambda}^{\text{HII}}$, $\hat{\tau}_{\lambda}^{\text{HI}}$, and $\hat{\tau}_{\lambda}^{\text{ISM}}$. For non-ionizing photons (with $\lambda > \lambda_L = 912 \text{ \AA}$), we thus write

$$T_{\lambda}^{\text{HII}} = \exp(-\hat{\tau}_{\lambda}^{\text{HII}}), \quad (8)$$

$$T_{\lambda}^{\text{HI}} = \exp(-\hat{\tau}_{\lambda}^{\text{HI}}), \quad (9)$$

$$T_{\lambda}^{\text{ISM}} = \exp(-\hat{\tau}_{\lambda}^{\text{ISM}}). \quad (10)$$

For some purposes, it is also convenient to define the total effective absorption optical depth of dust in the birth clouds and the fraction of this contributed by the internal HII regions

$$\hat{\tau}_{\lambda}^{\text{BC}} = \hat{\tau}_{\lambda}^{\text{HII}} + \hat{\tau}_{\lambda}^{\text{HI}}, \quad (11)$$

$$f = \hat{\tau}_{\lambda}^{\text{HII}} / (\hat{\tau}_{\lambda}^{\text{HII}} + \hat{\tau}_{\lambda}^{\text{HI}}). \quad (12)$$

We note that f may or may not coincide with the ratio of the HII to total gas column densities of the birth clouds, depending on whether or not the dust-to-gas ratios in the HII regions are the same as those in the HI regions.

Finally, we assume that the emission lines are produced only in the HII regions of the birth clouds. The justification for this is that the lifetimes of the birth clouds are generally greater than the lifetimes of the stars producing most of the ionizing photons, i.e. about 3×10^6 yr. In this case, line photons are absorbed in the HI regions and the ambient ISM in the same way as non-ionizing continuum photons. The emergent luminosity of a line of wavelength λ_l is thus

$$L_l(t) = \int_0^{t_{\text{BC}}} dt' \psi(t-t') S_l(t') T_{\lambda_l}^{\text{HI}} T_{\lambda_l}^{\text{ISM}}, \quad (13)$$

where $S_l(t')$ is the luminosity of the line produced in the HII regions by a stellar generation of age t' , and $T_{\lambda_l}^{\text{HI}}$ and $T_{\lambda_l}^{\text{ISM}}$ are given by equations (9) and (10). The luminosities of H-recombination lines are proportional to the ionization rate,

$$\dot{N}_{\text{ion}} = \frac{T_{\text{ion}}}{hc} \int_0^{\lambda_L} d\lambda \lambda S_{\lambda}, \quad (14)$$

where T_{ion} is the fraction of Lyman continuum photons absorbed by the gas rather than the dust in the HII regions. We adopt the formula

$$T_{\text{ion}} = \frac{(\hat{\tau}_{\lambda_L}^{\text{HII}})^3 \exp(-\hat{\tau}_{\lambda_L}^{\text{HII}})}{3\{(\hat{\tau}_{\lambda_L}^{\text{HII}})^2 - 2\hat{\tau}_{\lambda_L}^{\text{HI}} + 2[1 - \exp(-\hat{\tau}_{\lambda_L}^{\text{HII}})]\}}. \quad (15)$$

This equation, which is equivalent to equation (5-29) and Table 5.4 of Spitzer (1978), was derived by Petrosian, Silk, & Field (1972) and shown by them to provide a good approximation to the results of more detailed numerical computations.

We are especially interested in the emergent luminosities of the H α and H β Balmer lines of hydrogen, $L_{\text{H}\alpha}$ and $L_{\text{H}\beta}$. We assume that, given \dot{N}_{ion} , the production rates of all H-recombination photons are the same as for the dust-free case B recombination. This is validated by detailed photoionization models of HII regions, including the effects of

internal dust (Hummer & Storey 1992; Ferland 1996; Bottorff et al. 1998). For electronic densities $n_e \ll 10^4 \text{ cm}^{-3}$ and temperatures $T_e \approx 10^4 \text{ K}$, we then have (Osterbrock 1989)

$$\begin{aligned} S_{\text{H}\alpha} &= 0.450 (hc/\lambda_{\text{H}\alpha}) \dot{N}_{\text{ion}}, \\ S_{\text{H}\beta} &= 0.117 (hc/\lambda_{\text{H}\beta}) \dot{N}_{\text{ion}}, \end{aligned} \quad (16)$$

with $\lambda_{\text{H}\alpha} = 6563 \text{ \AA}$ and $\lambda_{\text{H}\beta} = 4861 \text{ \AA}$. It is straightforward to extend this procedure to compute the luminosity of any other H-recombination line (e.g., $\text{P}\beta$, $\text{B}\gamma$). We assume that all the power radiated in the form of $\text{L}\alpha$ photons, $\tilde{S}_{\text{L}\alpha} = 0.676 (hc/\lambda_{\text{L}\alpha}) \dot{N}_{\text{ion}}$, is eventually absorbed by dust as a consequence of resonant scattering ($\lambda_{\text{L}\alpha} = 1216 \text{ \AA}$). We have checked that our conclusions are not affected even if a significant fraction of $\text{L}\alpha$ photons escapes from the galaxy. For completeness, we compute the power from ionizing radiation that is neither absorbed by dust nor emerges in the $\text{H}\alpha$ and $\text{H}\beta$ lines,

$$S_X = \left(T_{\text{ion}} \int_0^{\lambda_L} d\lambda S_\lambda \right) - \left(\tilde{S}_{\text{L}\alpha} + S_{\text{H}\alpha} + S_{\text{H}\beta} \right), \quad (17)$$

and distribute this uniformly in wavelength between 3000 and 6000 \AA (a range that includes most of the relevant emission lines). This is only a few percent of all the stellar radiation and has a negligible influence on our results.

We now consider how the transmission function of the ambient ISM depends on the spatial distribution and optical properties of the dust. A particularly enlightening way to express T_λ^{ISM} is in terms of the probability density for the absorption of photons emitted in all directions by all stars within a galaxy. We define τ_λ as the optical depth of absorption along the path of a photon, from its emission by a star to its escape from the galaxy, including the influence of scattering on the path. From now on, we refer to τ_λ simply as the ‘‘optical depth’’ of the dust.³ We further define $p(\tau_\lambda)d\tau_\lambda$ as the probability that the optical depth lies between τ_λ and $\tau_\lambda + d\tau_\lambda$. Integrating over rays emanating in all directions from all stars within the galaxy, we can then write the transmission function of the ambient ISM as

$$T_\lambda^{\text{ISM}} = \int_0^\infty d\tau_\lambda p(\tau_\lambda) \exp(-\tau_\lambda). \quad (18)$$

If the spatial distribution of the dust is specified, this determines $p(\tau_\lambda)$, and T_λ^{ISM} then follows from equation (18). For some purposes, however, it is more informative to specify $p(\tau_\lambda)$ itself rather than any of the spatial distributions of the dust that could give rise to it when evaluating T_λ^{ISM} .

The optical depth τ_λ of the dust depends on a combination of absorption and scattering. If scattering were only in the forward direction, τ_λ would equal the true absorption optical depth. In the case of isotropic scattering, τ_λ is given by the geometrical mean of the true absorption and extinction (absorption plus scattering) optical depths, i.e.,

$$\tau_\lambda = [\tau_\lambda^a(\tau_\lambda^a + \tau_\lambda^s)]^{1/2} = \tau_\lambda^a(1 - \omega_\lambda)^{-1/2}, \quad (19)$$

where ω_λ is the single-scattering albedo (Rybicki & Lightman 1979).⁴ Although this formula was derived for an infinite homogeneous medium, it also provides an excellent approximation for more complicated geometries (see, e.g.,

Fig. 5 of Silva et al. 1998, which compares this approximation with a Monte Carlo calculation by Witt, Thronson, & Capuano 1992). In reality, both observations and models suggest that interstellar dust in the Milky Way has pronounced forward scattering at ultraviolet and optical wavelengths (e.g., Draine & Lee 1984; Kim, Martin, & Hendry 1994; Calzetti et al. 1995). Thus, we expect the truth to lie between the idealized formulae $\tau_\lambda = \tau_\lambda^a$ and $\tau_\lambda = \tau_\lambda^a(1 - \omega_\lambda)^{-1/2}$. In our model, the details of scattering and absorption are subsumed in our approximation of the optical depth of the dust as a power law in wavelength, $\tau_\lambda \propto \lambda^{-m}$ (§4). This approach would be questionable if we wished to compute directional quantities such as surface brightnesses. However, since we compute only angle-averaged quantities (i.e., luminosities), our simple treatment of scattering should be an adequate approximation. The reason for this is that, since many of the photons scattered out of a line of sight will be replaced by other photons scattered into it, inaccuracies in the treatment of scattering will partially (but not totally) cancel out when the emission is averaged over all directions.

We now consider three specific, idealized distributions of dust in the ambient ISM: a uniform foreground screen, a mixed slab, and discrete clouds. These are fairly standard representations, which may be regarded as illustrative of a wide range of possibilities. Other models could be constructed for more realistic and hence more complicated distributions of dust, for example by multiplying the transmission functions derived from different $p(\tau_\lambda)$'s. It should be recalled in any case that the total transmission function in our model is the product of that for the birth clouds and that for the ambient ISM, as specified by equation (6).

Foreground screen. The simplest model is that of a uniform foreground screen, which absorbs the light from all stars by the same amount. While unrealistic, this model has been adopted in many previous studies, and we include it here for reference. We call τ_λ^{sc} the optical depth of the screen. We then have

$$p(\tau_\lambda) = \delta(\tau_\lambda - \tau_\lambda^{\text{sc}}), \quad (20)$$

$$T_\lambda^{\text{ISM}} = \exp(-\tau_\lambda^{\text{sc}}), \quad (21)$$

where δ is the Dirac delta function.

Mixed slab. A potentially more realistic model is that of a slab filled with a uniform mixture of sources and absorbers (i.e., stars and dust). This can account for differences in the absorption affecting stars near the midplane or near the surface of a galactic disk. We call τ_λ^{sl} the full optical depth through the slab in the direction normal to the surface. By considering sources located at all points within the slab and rays emanating at all angles from the normal, we obtain, after some manipulation,

$$p(\tau_\lambda) = \begin{cases} 1/(2\tau_\lambda^{\text{sl}}), & \text{for } \tau_\lambda \leq \tau_\lambda^{\text{sl}}, \\ \tau_\lambda^{\text{sl}}/(2\tau_\lambda^2), & \text{for } \tau_\lambda > \tau_\lambda^{\text{sl}}, \end{cases} \quad (22)$$

$$T_\lambda^{\text{ISM}} = \frac{1}{2\tau_\lambda^{\text{sl}}} [1 + (\tau_\lambda^{\text{sl}} - 1) \exp(-\tau_\lambda^{\text{sl}}) - (\tau_\lambda^{\text{sl}})^2 E_1(\tau_\lambda^{\text{sl}})], \quad (23)$$

where E_1 is the exponential integral of the first order.

³The optical depth denoted here by τ_λ is sometimes referred to as an effective optical depth and denoted by τ_* (Rybicki & Lightman 1979). In this paper, we use the term ‘‘effective optical depth’’ to refer to the geometry-dependent optical depth $\hat{\tau}_\lambda$ defined by equation (4).

⁴Equation (19) is exact in the limit of large extinction optical depths but overestimates τ_λ in the opposite limit.

Discrete clouds. Both the foreground screen and mixed slab models are based on smooth representations of the ambient ISM. In real galaxies, however, the ISM is organized into clouds and other structures. The photons emitted in different directions by different stars can encounter any number of these clouds on their way out of the galaxy. Thus, $p(\tau_\lambda)$ may be better approximated by a Poisson distribution (Spitzer 1978; Natta & Panagia 1984). We call τ_λ^c the optical depth per cloud, and \bar{n} the mean number of clouds encountered along different lines of sight. The mean optical depth is thus $\bar{\tau}_\lambda = \bar{n}\tau_\lambda^c$. In this case, we have⁵

$$p(\tau_\lambda) = \sum_{n=0}^{\infty} \frac{\bar{n}^n}{n!} \exp(-\bar{n}) \delta(\tau_\lambda - n\tau_\lambda^c), \quad (24)$$

$$T_\lambda^{\text{ISM}} = \exp \left[-\bar{n}(1 - e^{-\tau_\lambda^c}) \right]. \quad (25)$$

In the limits $\tau_\lambda^c \rightarrow 0$ and $\tau_\lambda^c \rightarrow \infty$, we obtain the familiar expressions $T_\lambda^{\text{ISM}} \rightarrow \exp(-\bar{\tau}_\lambda)$ and $T_\lambda^{\text{ISM}} \rightarrow \exp(-\bar{n})$. This model should provide an adequate description of the absorption along individual random lines of sight, as required by equation (18), but it neglects possible correlations between the absorption along multiple nearby lines of sight, which may be important in other applications.

In principle, we could compute models with arbitrary star formation rates. For simplicity, in all the following applications, we take the star formation rate to be constant and include the age t of the stellar population as a parameter. This should be regarded as the effective age of the most recent burst of star formation, which can range from a few times 10^7 yr for a galaxy in an active starburst to several times 10^9 yr for a more quiescent galaxy. With the assumption $\psi = \text{const}$, equations (3), (4), and (6)–(11) allow us to reexpress the effective absorption optical depth at the time t in terms of the effective absorption optical depths in the birth clouds and the ISM as

$$\hat{\tau}_\lambda(t) = \hat{\tau}_\lambda^{\text{BC}} + \hat{\tau}_\lambda^{\text{ISM}} + \Delta\hat{\tau}_\lambda(t), \quad (26)$$

with

$$\Delta\hat{\tau}_\lambda(t) = \begin{cases} 0, & \text{for } t \leq t_{\text{BC}}, \\ -\ln \left[\frac{\int_0^{t_{\text{BC}}} dt' S_\lambda(t') + e^{\hat{\tau}_\lambda^{\text{BC}}} \int_{t_{\text{BC}}}^t dt' S_\lambda(t')}{\int_0^t dt' S_\lambda(t')} \right], & \text{for } t > t_{\text{BC}}. \end{cases} \quad (27)$$

We compute $S_\lambda(t')$ using the latest version of the Bruzual & Charlot (1993) population synthesis code. Our conclusions would not be affected by the use of other standard codes. Unless otherwise indicated, we adopt solar metallicity and a Salpeter IMF truncated at 0.1 and $100 M_\odot$.

We now have a completely specified model for the absorption of starlight by dust in galaxies. The main adjustable parameters describing the birth clouds are: the lifetime of the clouds, t_{BC} ; the wavelength dependence and normalization of $\hat{\tau}_\lambda^{\text{BC}}$; and the fraction of $\hat{\tau}_\lambda^{\text{BC}}$ contributed by dust in HII regions, f . For the ambient ISM, the parameters depend on whether we adopt a foreground screen model (τ_λ^{sc}), a mixed slab model (τ_λ^{sl}), or a discrete cloud

model (τ_λ^c and \bar{n}). The other main parameter is the effective age of the starburst, t . We compute the continuum luminosity per unit wavelength emerging from a galaxy using equations (1) and (6)–(10). The emergent H α and H β line luminosities, $L_{\text{H}\alpha}(t)$ and $L_{\text{H}\beta}(t)$, are obtained from equations (9), (10), and (13)–(16). The ratio of the H α line and continuum luminosities is then the emission equivalent width of the emergent H α line, $W_{\text{H}\alpha}(t)$. Finally, we compute the far-infrared luminosity of the galaxy, $L_{\text{dust}}(t)$, using equations (3) and (5).

In the remainder of this paper, we take two approaches to compare our model with observations. As equations (10) and (18) indicate, the optical properties and spatial distribution of the dust affect observable quantities only through the effective absorption curve $\hat{\tau}_\lambda^{\text{ISM}}$. Different combinations of τ_λ and $p(\tau_\lambda)$, however, could lead to the same wavelength dependence of $\hat{\tau}_\lambda^{\text{ISM}}$. Thus, it is of primary interest to study how the wavelength dependence of $\hat{\tau}_\lambda^{\text{ISM}}$ is constrained by observations. This is our goal in §3 below. Then, in §4, we explore whether there are examples of optical properties and spatial distributions of the dust that satisfy these constraints, recognizing that there is no unique solution.

3. COMPARISONS WITH OBSERVATIONS: THE EFFECTIVE ABSORPTION CURVE

In this section, we use observations of nearby starburst galaxies to constrain the wavelength dependence of the effective absorption curve $\hat{\tau}_\lambda$ defined by equation (4) without specifying the spatial distribution and optical properties of the dust. We also identify the specific influence of each parameter in the model on different integrated spectral properties of galaxies and investigate the physical origin of the observed relationships between these properties. We assume for simplicity that the effective absorption curves of the birth clouds and the ambient ISM have the same power-law form,

$$\hat{\tau}_\lambda^{\text{BC}} = \hat{\tau}_V^{\text{BC}} (\lambda/5500 \text{ \AA})^{-n}, \quad (28)$$

$$\hat{\tau}_\lambda^{\text{ISM}} = \hat{\tau}_V^{\text{ISM}} (\lambda/5500 \text{ \AA})^{-n}, \quad (29)$$

where n is a parameter to be determined, and $\hat{\tau}_V^{\text{BC}}$ and $\hat{\tau}_V^{\text{ISM}}$ are the normalizing coefficients at 5500 Å.

To calibrate our model, we appeal to a homogeneous set of observations of nearby ultraviolet-selected starburst galaxies, for which the ultraviolet, far-infrared, H α , and H β fluxes, H α equivalent widths, and ultraviolet spectral slopes are available. The sample, compiled by Meurer et al. (1999), includes 57 non-Seyfert galaxies from the *International Ultraviolet Explorer (IUE)* atlas of Kinney et al. (1993) classified into one of the starburst categories (i.e., starburst nucleus, starburst ring, blue compact dwarf galaxy, or blue compact galaxy). This sample has been further restricted by Meurer et al. (1999) to galaxies with optical angular diameters less than 4', for which most of the (usually concentrated) ultraviolet emission could be observed within the *IUE* aperture. The galaxies span a wide range of morphological types, from Sab to Irr, and a wide range of absolute B -band magnitudes, $-16 \lesssim M_B \lesssim -22$ (we adopt a Hubble constant $H_0 = 70 \text{ km s}^{-1} \text{ Mpc}^{-1}$).

⁵Strictly, equation (24) corresponds to a Poisson distribution of identical, face-on screens. For spherical clouds, the factor $\delta(\tau_\lambda - n\tau_\lambda^c)$ would have to be replaced by a function with a finite width to account for the different optical depths seen by photons with different impact parameters. We ignore this subtlety here.

From the *IUE* spectra of all galaxies in the sample, Meurer et al. (1999) compute the restframe ultraviolet flux at 1600 Å, F_{1600} , and the slope β of the ultraviolet continuum. The quantity F_{1600} is defined as λf_λ , where f_{1600} is the mean flux density over a square passband with a central wavelength of 1600 Å and a width of 350 Å. The slope β is determined from a power-law fit of the form $f_\lambda \propto \lambda^\beta$ to the observed ultraviolet spectrum in ten continuum bands that avoid strong stellar and interstellar absorption features (in particular, the 2175 Å dust feature) in the range $1268 \leq \lambda \leq 2580$ Å, as defined by Calzetti et al. (1994). These ultraviolet properties were derived for galaxies in the sample after removing foreground extinction by the Milky Way.

Observations with the *Infrared Astronomical Satellite* (*IRAS*) are available for 47 galaxies in the sample. To estimate the total far-infrared flux F_{dust} from the observed *IRAS* flux densities, $f_\nu(60 \mu\text{m})$ and $f_\nu(100 \mu\text{m})$, we follow the prescription of Meurer et al. (1999). They first calculate the quantity $F_{\text{FIR}} = 1.26 \times 10^{-11} [2.58 f_\nu(60 \mu\text{m}) + f_\nu(100 \mu\text{m})]$ ergs cm⁻²s⁻¹ defined by Helou et al. (1988) and then compute F_{dust} (F_{bol} in their notation) from F_{FIR} and $f_\nu(60 \mu\text{m})/f_\nu(100 \mu\text{m})$ using the bolometric correction appropriate for dust with a single temperature and an emissivity proportional to frequency ν . This prescription agrees reasonably well with observations from near-infrared to submillimeter wavelengths for a small sample of galaxies (see Fig. 2 of Meurer et al. 1999). The corrections from F_{FIR} to F_{dust} are relatively small, with a mean $\langle F_{\text{dust}}/F_{\text{FIR}} \rangle \approx 1.4$ and a standard deviation of 0.1. Finally, for 31 galaxies, the ratio of H α to H β fluxes and the H α equivalent width are available from Storchi-Bergmann, Kinney, & Challis (1995) and McQuade, Calzetti, & Kinney (1995), with corrections for stellar absorption by Calzetti et al. (1994). Neglecting possible anisotropies, we equate flux ratios at all wavelengths to the corresponding luminosity ratios. Figures 2, 3, and 4 show L_{dust}/L_{1600} , $L_{\text{H}\alpha}/L_{\text{H}\beta}$, and $W_{\text{H}\alpha}$, respectively, as a function of β for this sample. The typical scatter at fixed β amounts to a factor of about 2 in L_{dust}/L_{1600} and $L_{\text{H}\alpha}/L_{\text{H}\beta}$, but nearly a factor of 10 in $W_{\text{H}\alpha}$. Thus, both L_{dust}/L_{1600} and $L_{\text{H}\alpha}/L_{\text{H}\beta}$, to a first approximation, are functions of β , while there is little or no correlation between $W_{\text{H}\alpha}$ and β . We note, however, that the scatter even in the first two relations appears to be real because it is larger than the typical measurement errors (which are shown in the upper left panels of Figs. 2–4).

We now use these observations to constrain the parameters in our model. Our goal is to identify models that account for the typical properties, scatter, and trends seen in the sample, rather than to interpret in detail the emission from individual galaxies. Such an attempt might be of limited validity because the predictions of our model, unlike the observations, are averaged over angles.⁶ We have checked, however, that the properties of every galaxy in the sample could be reproduced with at least one combination of parameters. The influence of each parameter on observable quantities can best be explored by keeping all other parameters fixed at “standard” values. After some

experimentation, we adopted:

$$\begin{aligned} t &= 3 \times 10^8 \text{ yr} \\ t_{\text{BC}} &= 1 \times 10^7 \text{ yr} \\ \hat{\tau}_{\text{V}}^{\text{BC}} &= 1.0 \\ \hat{\tau}_{\text{V}}^{\text{ISM}} &= 0.5 \\ f &= 0.1 \\ n &= 0.7. \end{aligned} \quad (30)$$

While these values are not the results of a rigorous optimization procedure, they do enable the standard model to match roughly the observed typical (i.e., median) properties of the starburst sample. We note that $\hat{\tau}_{\text{V}}^{\text{BC}} \approx 1$ is typical of the observed optical depths to O-type and supergiant stars in the Milky Way (Humphreys 1978). The dense cores of molecular clouds have higher optical depths, but even short-lived stars spend only the first 10%–20% of their lifetimes in these regions (e.g., Mezger & Smith 1977). Also, $t_{\text{BC}} \approx 10^7$ yr is typical of the timescale for the dispersal of giant molecular clouds in the Milky Way (Blitz & Shu 1980).

We now compare the predictions of our model with the observations described above. Each panel in Figures 2–4 shows the effect of increasing and decreasing one parameter with respect to its standard value with the others held fixed. We can summarize the role of each parameter as follows.

Effective starburst age. The effect of increasing t is most noticeable on the H α equivalent width, which drops from almost 300 Å at $t = 3 \times 10^7$ yr to less than 100 Å at $t = 3 \times 10^8$ yr because of the rising contribution by old stars to the continuum near the line (Fig. 4a). Increasing t also makes the ultraviolet spectral slope larger because old stars have intrinsically red spectra. However, this does not affect the H α /H β ratio, since the emission lines are produced mainly by stars younger than about 3×10^6 yr (Fig. 3a).

Lifetime of the birth clouds. Increasing t_{BC} makes both β and the ratio of far-infrared to ultraviolet luminosities larger because the radiation from young blue stars is heavily absorbed for a longer time (Fig. 2b). Changes in t_{BC} do not affect $L_{\text{H}\alpha}/L_{\text{H}\beta}$ because we have assumed that the birth clouds last longer than 3×10^6 yr, the lifetime of stars producing most of the ionizing photons (§2). However, since more of the continuum luminosity near H α is absorbed for larger t_{BC} , the H α equivalent width also increases (Fig. 4b).

Effective absorption optical depth in the birth clouds. Increasing $\hat{\tau}_{\text{V}}^{\text{BC}}$ above unity has the remarkable property of making $L_{\text{H}\alpha}/L_{\text{H}\beta}$ larger at almost fixed β and L_{dust}/L_{1600} (Figs. 2c and 3c). The reason for this is that, while $L_{\text{H}\alpha}/L_{\text{H}\beta}$ traces the absorption in the HI envelopes of the birth clouds, the ultraviolet radiation from embedded stars is so attenuated for $\hat{\tau}_{\text{V}}^{\text{BC}} \gtrsim 1$ that L_{dust} saturates, and β and L_{1600} are dominated by stars in the ambient ISM. This has fundamental observational implications (see below). Figure 4c also shows that the H α equivalent width is very sensitive to changes in $\hat{\tau}_{\text{V}}^{\text{BC}}$, which affect $L_{\text{H}\alpha}$.

Effective absorption optical depth in the ambient ISM. Since $\hat{\tau}_{\text{V}}^{\text{ISM}}$ controls the absorption of stars that have emerged from their birth clouds, it has a major influence

⁶Although some differences are expected between the luminosity ratios and flux ratios due to anisotropic emission from galaxies, these must be relatively small or else the relations shown in Figures 2 and 3 would be washed out. The obvious outlier at $\beta = -0.76$ and $\log(L_{\text{dust}}/L_{1600}) = 2.2$ in Figure 2 could be a galaxy for which some of the ultraviolet emission was missed with *IUE* (see the discussion in §3.1 in Meurer et al. 1999).

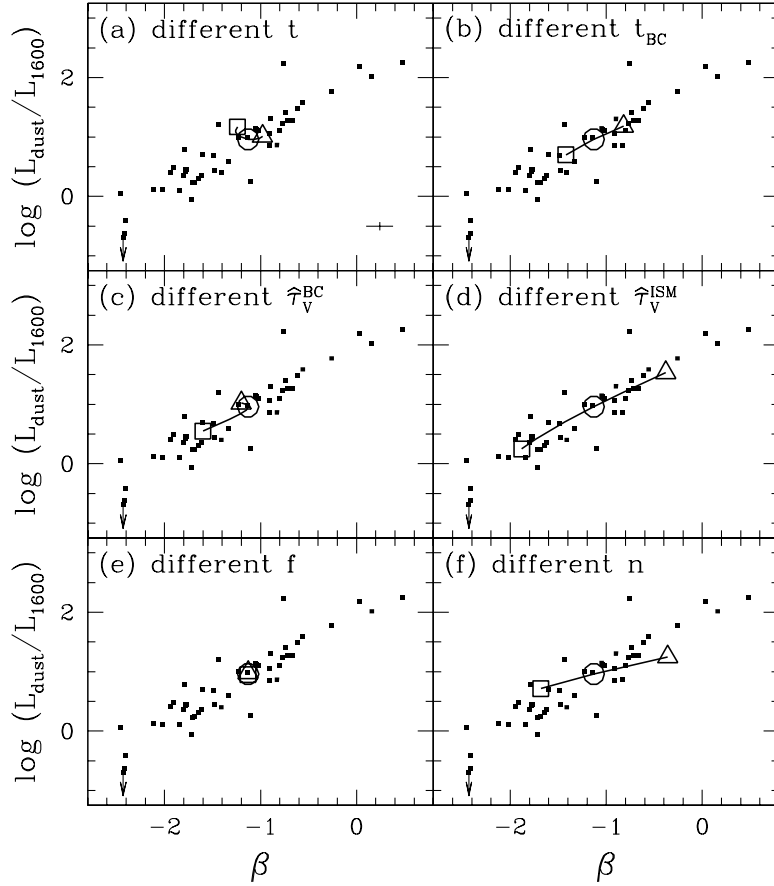


FIG. 2.— Ratio of far-infrared to ultraviolet luminosities plotted against ultraviolet spectral slope. The data points are from the Meurer et al. (1999) sample discussed in §3 and are repeated in all panels (typical measurement errors are indicated in the upper left panel). In each case, the line shows the effect of varying one parameter from the lower end of the range (*square*) to the standard value (*circle*) to the upper end of the range (*triangle*), with all other parameters fixed at their standard values (eq. [30]): (a) effective starburst ages, $t = 3 \times 10^7$, 3×10^8 , and 3×10^9 yr; (b) lifetimes of the birth clouds, $t_{\text{BC}} = 3 \times 10^6$, 1×10^7 , and 3×10^7 yr; (c) effective optical depths in the birth clouds, $\hat{\tau}_{\text{V}}^{\text{BC}} = 0.0, 1.0, \text{ and } 2.0$; (d) effective optical depths in the ambient ISM, $\hat{\tau}_{\text{V}}^{\text{ISM}} = 0.0, 0.5, \text{ and } 1.0$; (e) fractions of dust in HII regions in the birth clouds, $f = 0.0, 0.1, \text{ and } 1.0$; and (f) exponents in the relation $\hat{\tau}_{\lambda}^{\text{ISM}} \propto \lambda^{-n}$, $n = 0.4, 0.7, \text{ and } 1.0$.

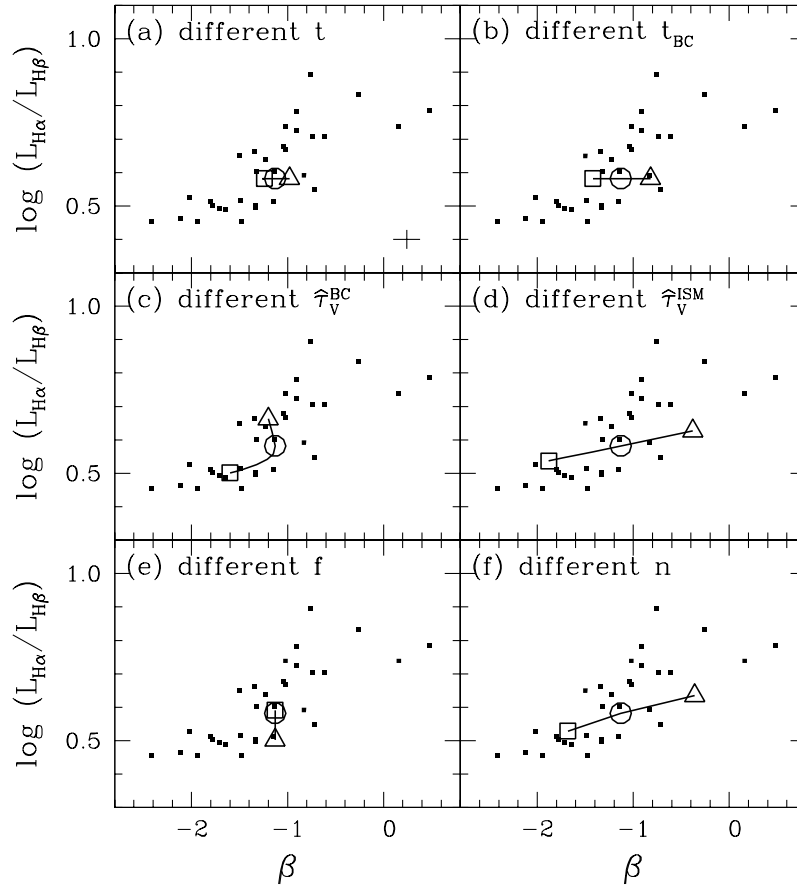


FIG. 3.— $H\alpha/H\beta$ ratio plotted against ultraviolet spectral slope. The data points are from the Meurer et al. (1999) sample discussed in §3 and are repeated in all panels (typical measurement errors are indicated in the upper left panel). In each case, the line shows the effect of varying one parameter from the lower end of the range (*square*) to the standard value (*circle*) to the upper end of the range (*triangle*), with all other parameters fixed at their standard values (eq. [30]). The models are the same as in Fig. 2.

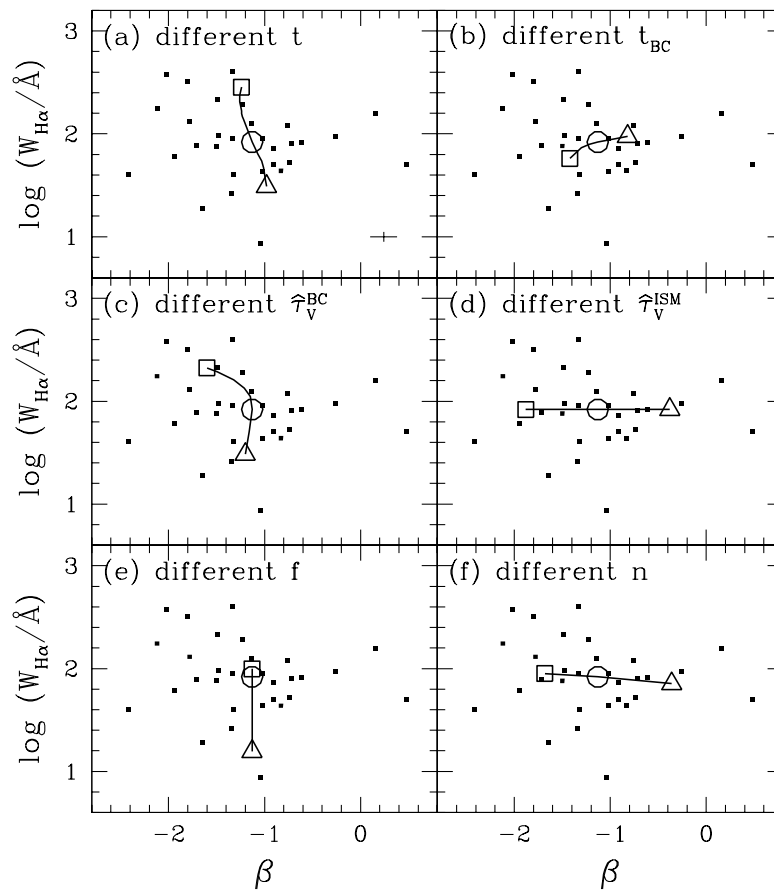


FIG. 4.— H α equivalent width plotted against ultraviolet spectral slope. The data points are from the Meurer et al. (1999) sample discussed in §3, with H α equivalent widths from Storchi-Bergmann et al. (1995) and McQuade et al. (1995), and are repeated in all panels (typical measurement errors are indicated in the upper left panel). In each case, the line shows the effect of varying one parameter from the lower end of the range (*square*) to the standard value (*circle*) to the upper end of the range (*triangle*), with all other parameters fixed at their standard values (eq. [30]). The models are the same as in Fig. 2.

on the ultraviolet spectra and hence on β and L_{dust}/L_{1600} (Fig. 2d). Changes in $\hat{\tau}_V^{\text{ISM}}$ also affect the $\text{H}\alpha/\text{H}\beta$ ratio, although with a strong dependence on β (Fig. 3d). As expected, $\hat{\tau}_V^{\text{ISM}}$ has no effect on $W_{\text{H}\alpha}$.

Fraction of dust in the HII regions. Increasing f causes more ionizing photons to be absorbed by dust and hence reduces the $\text{H}\alpha$ equivalent width considerably (Fig. 4e). Dust in HII regions has a negligible effect on the $\text{H}\alpha/\text{H}\beta$ ratio. However, since we have kept $\hat{\tau}_V^{\text{BC}}$ fixed, increasing f reduces the absorption in the HI envelopes of the birth clouds and hence the $\text{H}\alpha/\text{H}\beta$ ratio in Figure 3e. Changes in f have no effect on β and L_{1600} and a negligible effect on L_{dust} .

Exponent of the effective absorption curve. Increasing n steepens the effective absorption curve. This increases the ratio of far-infrared to ultraviolet luminosities, the $\text{H}\alpha/\text{H}\beta$ ratio, and the ultraviolet spectral slope and reduces slightly the $\text{H}\alpha$ equivalent width (Figs. 2f–4f). We elaborate below on the reason for adopting $n = 0.7$ as a standard value.

Other parameters. We have also computed models with different IMFs and metallicities (not shown). Changes in these parameters have no influence on $L_{\text{H}\alpha}/L_{\text{H}\beta}$ and affect β and L_{dust}/L_{1600} at the level of less than 20%. The influence on the $\text{H}\alpha$ equivalent width is slightly stronger. For example, adopting a Scalo IMF instead of a Salpeter IMF would reduce $W_{\text{H}\alpha}$ by about 50% for the standard model because of the smaller proportion of massive stars. In contrast, adopting a metallicity 20% of the solar value would increase $W_{\text{H}\alpha}$ by about 20% because metal-poor stars are hotter than solar-metallicity stars. We also tested the influence of a possible leakage of some ionizing photons from HII regions into the ambient ISM by allowing 50% of the line photons produced by stars in the standard model to escape without absorption in the HI envelopes of the birth clouds (Oey & Kennicutt 1997, and references therein). While the $\text{H}\alpha/\text{H}\beta$ ratio was found to be only 12% lower in this case than in the standard model, the $\text{H}\alpha$ equivalent width increased by 60%.

It is also interesting to examine the shape of the total effective absorption curve defined by equation (4) and its dependence on the age of the stellar population. In Figure 5, we show $\hat{\tau}_\lambda(t)$ at different ages for our standard model (computed from eqs. [26] and [27]). Initially, for $t \leq t_{\text{BC}}$, $\hat{\tau}_\lambda$ is a power law of index $n = 0.7$. At later times, the effective absorption curve steepens markedly at wavelengths $\lambda \lesssim 1200 \text{ \AA}$ ($\log \lambda \lesssim 3.1$). It is more similar to the initial power law in the wavelength range where β is determined ($1200 \lesssim \lambda \lesssim 2500 \text{ \AA}$), but steeper again at wavelengths $\lambda \gtrsim 4000 \text{ \AA}$ ($\log \lambda \gtrsim 3.6$). The reason for this is that short-lived, massive stars, which produce most of the luminosity at $\lambda \lesssim 1200 \text{ \AA}$, are embedded in the birth clouds, where their radiation is heavily absorbed. Their contribution is substantial and nearly constant across the wavelength range $1200 \lesssim \lambda \lesssim 2500 \text{ \AA}$ but less important at longer wavelengths. The steepening of $\hat{\tau}_\lambda$ at $\lambda \gtrsim 4000 \text{ \AA}$ is also enhanced by the appearance in the ambient ISM of long-lived stars with a strong 4000 \AA break in their spectra, which contribute more light redward than blueward of the break. The absorption in the birth clouds, therefore, has a major influence on the shape of the effective absorption curve.

It is worth pausing here to emphasize the important implications of the finite lifetimes of the birth clouds. As mentioned in §1, emission lines appear to be more attenuated than the continuum radiation in starburst galaxies. This led Calzetti (1997) to suggest that ultraviolet-bright stars must be somehow physically detached from the gas they ionize. In our model, the lines produced in HII regions and the non-ionizing continuum radiation from young stars are attenuated in the same way by dust in the outer HI envelopes of the birth clouds and the ambient ISM. However, since the birth clouds have finite lifetimes, the non-ionizing continuum radiation from stars that live longer than the birth clouds is attenuated only by the ambient ISM. The ultraviolet and optical continuum radiation, therefore, appears to be less attenuated than the lines. This can be seen clearly in Figures 3c and 4c from the rise in the $\text{H}\alpha/\text{H}\beta$ ratio accompanying the drop in the $\text{H}\alpha$ equivalent width at nearly constant ultraviolet spectral slope as the effective absorption optical depth of the birth clouds increases above unity. Thus, the finite lifetime of the birth clouds is a key ingredient to resolve the apparent discrepancy between the attenuation of line and continuum photons in starburst galaxies.

Since each parameter in our model has a specific influence on the various integrated spectral properties of starburst galaxies, we can gain insight into the physical origin of the relations defined by these observed quantities. An inspection of Figures 2–4 leads to the following conclusions. (1) The wide observed range of ultraviolet spectral slopes can be most naturally understood as a spread in the effective absorption optical depth in the ambient ISM, although variations in the lifetimes of the birth clouds could also play some role. It is worth mentioning that the steep ultraviolet spectra of the galaxies with largest β cannot originate from old stars because these galaxies also have large $W_{\text{H}\alpha}$. (2) As noted above, absorption in the birth clouds is required to explain the large $\text{H}\alpha/\text{H}\beta$ ratios observed in galaxies with intermediate ultraviolet spectral slopes. (3) The fact that L_{dust}/L_{1600} , $L_{\text{H}\alpha}/L_{\text{H}\beta}$, and β are all very low at one end of the observed relations and all very high at the other end further suggests that variations in the effective optical depths of the birth clouds and the ambient ISM may be related (Figs. 2 and 3). To explore the effects of varying simultaneously $\hat{\tau}_V^{\text{BC}}$ and $\hat{\tau}_V^{\text{ISM}}$, we assume that they are related by $\hat{\tau}_V^{\text{BC}} = 2\hat{\tau}_V^{\text{ISM}}$ and fix all other parameters at the standard values given by equation (30). The results are shown in Figure 6. Evidently, the models reproduce well the observed relations between L_{dust}/L_{1600} , $L_{\text{H}\alpha}/L_{\text{H}\beta}$, and β in Figures 6a and 6b. They also fall roughly in the middle of the observed ranges of $W_{\text{H}\alpha}$ and β in Figure 6c.

An important result of our analysis is that the shape of the relation between L_{dust}/L_{1600} and β actually *requires* that the exponent of the effective absorption curve $\hat{\tau}_\lambda^{\text{ISM}} \propto \lambda^{-n}$ be $n \approx 0.7$. In Figure 6, we also show models with $\hat{\tau}_V^{\text{BC}} = 2\hat{\tau}_V^{\text{ISM}}$ as above, but for $n = 0.4$ and 1.0 instead of 0.7 . These models miss the observed relation, the sequence being too steep for $n = 0.4$ and too shallow for $n = 1.0$. This observational constraint on n applies essentially to $\hat{\tau}_\lambda^{\text{ISM}}$, since L_{dust}/L_{1600} and β are almost independent of $\hat{\tau}_\lambda^{\text{BC}}$ for $\hat{\tau}_\lambda^{\text{BC}} \gtrsim 1$. For $n = 0.7$, therefore, the relations defined by L_{dust}/L_{1600} , $L_{\text{H}\alpha}/L_{\text{H}\beta}$, and β can

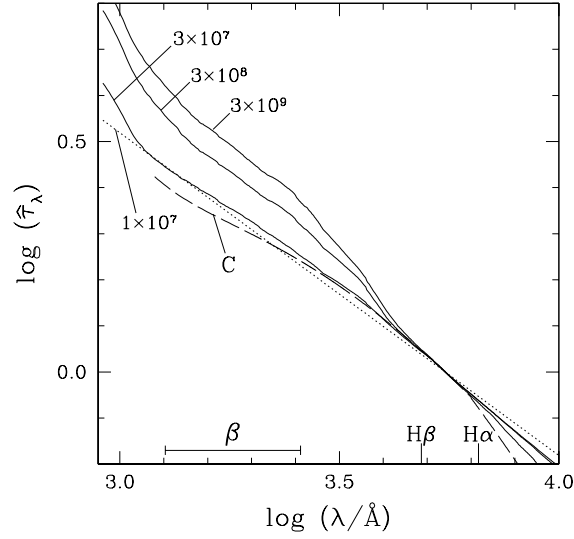


FIG. 5.— Effective absorption curve (as defined by eq. [4]) of our standard model at different effective starburst ages, as indicated. The dashed curve is from Calzetti et al. (1994). For reference, the wavelength range where the ultraviolet slope β is determined and the wavelengths of the H α and H β lines are indicated at the bottom. All curves are normalized to unity at 5500 Å.

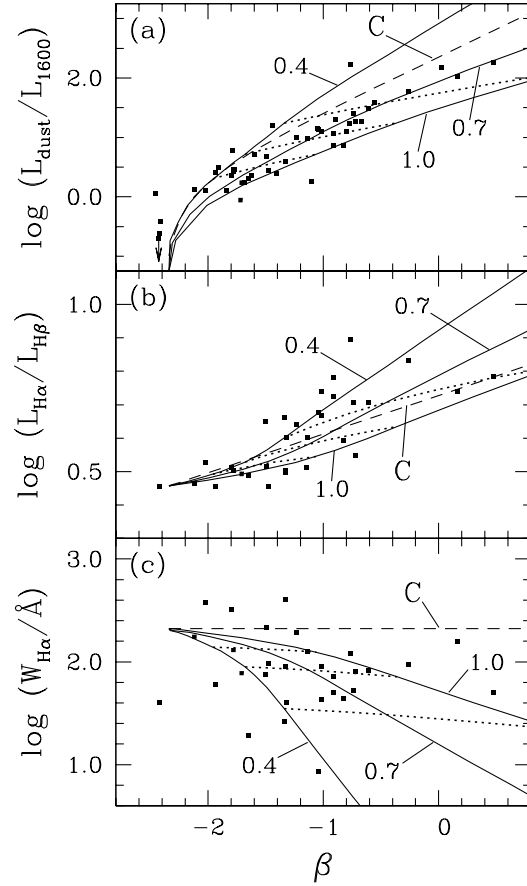


FIG. 6.— Sequences of models with different dust content and $\hat{\tau}_V^{BC} = 2\hat{\tau}_V^{ISM}$. The solid curves correspond to different exponents n in the relation $\hat{\tau}_\lambda^{ISM} \propto \lambda^{-n}$ (as indicated). Dotted lines join models with $\hat{\tau}_V^{BC} = 0.5, 1.0, \text{ and } 2.0$ (in order of increasing β) to indicate the scale. The dashed curve is a sequence of models with $\hat{\tau}_V^{BC} = 0.0$ and $\hat{\tau}_\lambda^{ISM}$ from Calzetti et al. (1994). The data points in (a), (b), and (c) are the same as in Figs. 2, 3, and 4, respectively.

be understood most simply as a sequence in the overall dust content of galaxies. Our assumption of $\hat{\tau}_V^{\text{BC}} = 2\hat{\tau}_V^{\text{ISM}}$ should be taken merely as illustrative. With $n = 0.7$, the observations can be matched by a variety of models that range from $\hat{\tau}_V^{\text{BC}} + \hat{\tau}_V^{\text{ISM}} = 0$ at one end of the relations (with $\beta = -2.3$) to $\hat{\tau}_V^{\text{BC}} \gtrsim 1.0$ and $\hat{\tau}_V^{\text{ISM}} \approx 1.5$ at the other end (with $\beta \approx +0.2$). For reference, the fraction of the total stellar radiation absorbed by dust in the models of Figure 6 ranges from 0% to about 90% along this sequence and is roughly 70% for our standard model. Non-ionizing continuum photons account for about 90% of the heating in all models except for those with very low dust content, in which the relative contribution by Ly α photons is more important (over 20% for $\beta \lesssim -2.2$). As Figures 2–4 indicate, the intrinsic scatter about the relations at fixed β can arise from variations in the effective age of the starburst, the parameters controlling the birth clouds, and the fraction of dust in the HII regions (and possibly the IMF and metallicity of the stars).

Our models are also consistent with observations of near-infrared H-recombination lines in starburst galaxies. The fluxes of the Paschen β (1.28 μm) and Brackett γ (2.17 μm) lines of 11 galaxies in the Meurer et al. (1999) sample are available from Calzetti et al. (1996). We compute the P β and B γ luminosities, $L_{\text{P}\beta}$ and $L_{\text{B}\gamma}$, using the same procedure as described in §2 for $L_{\text{H}\alpha}$ and $L_{\text{H}\beta}$. Figure 7 shows the H β /B γ and P β /B γ ratios as a function of the H α /H β ratio for the observations and for the same models as in Figure 6. Sequences of models are straight lines in these log-log diagrams, reflecting the assumed power-law form of the effective absorption curves in the birth clouds and the ambient ISM. Figure 7 shows that $n = 0.7$ is consistent with, although not tightly constrained by, the observed strengths of optical and near-infrared recombinations lines in nearby starburst galaxies. As noted above, the exponent n of the effective absorption curve is much better constrained by the relation between the ratio of far-infrared to ultraviolet luminosities and the ultraviolet spectral slope.

It is worth noting that the observed mean relations can be reproduced by the following simple recipe: use an effective absorption curve proportional to $\lambda^{-0.7}$ to attenuate the non-ionizing continuum radiation and emission lines (as predicted by dust-free case B recombination) from each stellar generation, and lower the normalization of the curve typically by a factor of 3 after 10^7 yr to account for the dispersal of the birth clouds. This recipe approximates the results of our full calculations shown in Figures 6 and 7 but differs from them in that it omits the absorption of ionizing photons by dust in HII regions (i.e., it assumes $f = 0.0$). As mentioned earlier, this has no effect on the ultraviolet spectrum and a negligible effect on the far-infrared luminosity ($< 1\%$ underestimate) and the H α /H β ratio (from $< 1\%$ to about 7% overestimate along the observed relations). The effect is more important for the H α equivalent width (from 3% to over 70% overestimate). Of course, the simple recipe above does not allow one to reproduce the scatter in the observed relations, which requires variations

in several parameters of our model. However, if only the mean properties are considered, the simple recipe should suffice for many purposes. Both our complete model and the simple recipe derived from it can be incorporated easily into any population synthesis model.

In an attempt to understand the physical basis for the observed relation between L_{dust}/L_{1600} and β , we plot other properties of the galaxies against β in Figure 8: the oxygen abundance of HII regions O/H and the absolute B magnitude M_B . The oxygen abundances of 31 galaxies of the Meurer et al. (1999) sample, measured in the same aperture as β , are available from Calzetti et al. (1994), while the absolute B magnitudes of all the galaxies are available from Kinney et al. (1993). The Spearman rank correlation coefficients are $r_s = 0.76$ for the relation between O/H and β and $r_s = -0.50$ for that between M_B and β . For the different numbers of galaxies in each case, these correlations are significant at the 4σ and 3σ levels. Thus, they are probably both statistically significant, especially the one between O/H and β (which was noted by Calzetti et al. 1994 from a slightly different sample), but both have very large scatter. This suggests that neither O/H nor M_B are entirely responsible for the relations between L_{dust}/L_{1600} , $L_{\text{H}\alpha}/L_{\text{H}\beta}$, and β . The ultimate physical explanation for these relations therefore requires further investigation.

For reference, we have also computed models using the Calzetti et al. (1994) effective absorption curve. This was derived from the analysis of *IUE* spectra of a sample of 33 starburst galaxies, nearly all of which are included in the Meurer et al. (1999) sample. Calzetti et al. (1994) condensed all the spectra in their sample into six “templates” corresponding to different values of the H α /H β ratio. They then derived an effective absorption curve by dividing the five spectral templates with the highest $L_{\text{H}\alpha}/L_{\text{H}\beta}$ by the template with the lowest $L_{\text{H}\alpha}/L_{\text{H}\beta}$ (assuming that the latter represented the dust-free case). The result is strictly an effective absorption curve in the sense defined by equation (4), although it is often referred to by other names (see footnote 2). Figure 5 shows that the Calzetti et al. (1994) effective absorption curve is greyer than those derived here. In Figure 6, we show the results obtained when adopting the Calzetti et al. (1994) curve for $\hat{\tau}_\lambda^{\text{ISM}}$ and assuming $\hat{\tau}_V^{\text{BC}} = 0$ for consistency.⁷ As anticipated, the models predict a steeper relation between L_{dust}/L_{1600} and β than is observed. The greyness of the Calzetti et al. (1994) curve probably results from a bias inherent in the method used to derive it. As Figure 6b shows, galaxies with the lowest observed H α /H β ratios extend over a fairly wide range of ultraviolet spectral slopes. Thus, the template spectrum with the lowest $L_{\text{H}\alpha}/L_{\text{H}\beta}$, built by Calzetti et al. (1994) from eight spectra with $-2.08 \leq \beta \leq -1.33$, may be relatively but not perfectly dust free, as is assumed by the method.

4. COMPARISONS WITH OBSERVATIONS: THE SPATIAL DISTRIBUTION OF DUST

Up to now, we have compared our model with observations only in terms of the effective absorption curve, i.e., without specifying the spatial distribution and op-

⁷To extend the Calzetti et al. (1994) curve into the near-infrared over the range $0.8 \leq \lambda \leq 2.2 \mu\text{m}$, we use the formula provided by Calzetti (1999). To compute $\hat{\tau}_\lambda^{\text{ISM}}$ at wavelengths $912 \leq \lambda \leq 1200 \text{ \AA}$, we extrapolate the curve linearly in $\log \lambda$. This has a negligible influence on the results because typically less than 25% of L_{dust} is produced by the absorption blueward of 1200 \AA . In fact, adopting $\hat{\tau}_\lambda^{\text{ISM}} \equiv \hat{\tau}_{1200}^{\text{ISM}}$ for $\lambda \leq 1200 \text{ \AA}$ gives similar results.

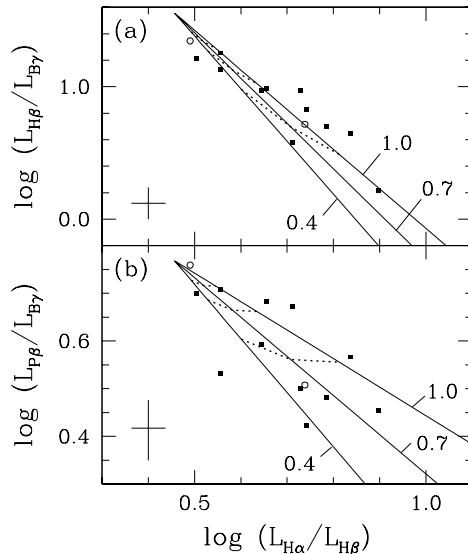


FIG. 7.— (a) $H\beta/B\gamma$ ratio and (b) $P\beta/B\gamma$ ratio plotted against $H\alpha/H\beta$ ratio. The data points are from Calzetti et al. (1996) and include 11 galaxies from the Meurer et al. (1999) sample (*filled squares*) plus two additional nearby starburst galaxies (*open circles*). The solid and dotted curves are the same models as in Fig. 6. Typical measurement errors are indicated in each panel.

tical properties of the dust. In this section, we study the influence of different spatial distributions of dust on the integrated spectral properties of galaxies. As shown in §3, the effective absorption curve favored by observations of nearby starburst galaxies is significantly shallower than most known extinction curves. This is a natural consequence of any spatial distribution of dust in which the least extinguished stars contribute most to the emergent light at short wavelengths. Such an effect has been quantified for many distributions of dust, both patchy and smooth (e.g., Natta & Panagia 1984; Caplan & Deharveng 1986; Bruzual, Magris, & Calvet 1988; Disney, Davies, & Phillipps 1989; Witt et al. 1992; Calzetti et al. 1994, 1996; Puxley & Brand 1994; Di Bartolomeo, Barbaro, & Perinotto 1995; Bianchi, Ferrara, & Giovanardi 1996; Witt & Gordon 1996; Gordon et al. 1997). These studies, however, did not include the finite lifetimes of stellar birth clouds. Thus, they cannot account for the different attenuation of line and continuum photons in starburst galaxies. We now investigate the influence of the spatial distribution of the dust on the effective absorption curve in the context of our model.

For simplicity, we assume that the optical depth of the dust has a power-law form

$$\tau_\lambda \propto \lambda^{-m}, \quad (31)$$

where the choice of m is discussed below. This is consistent with recent evidence that the optical depth of the dust in nearby starburst galaxies does not exhibit a strong feature near 2175 \AA (Gordon et al. 1997). We further assume for simplicity that $\hat{\tau}_\lambda^{\text{BC}}$ has the same wavelength depen-

dence as τ_λ . For comparison, Figure 9 shows τ_λ plotted against λ for Milky Way-type, LMC (30 Doradus)-type, and SMC-type dust and for the two cases of forward-only and isotropic scattering (eq. [19]). These optical properties are based on the standard Draine & Lee (1984) grain model but with the proportions of graphite and silicates adjusted so as to fit the observed mean extinction curves of the three galaxies (Pei 1992). The inclusion of scattering makes τ_λ greyer because the albedo is larger at optical than at ultraviolet wavelengths, the effect increasing from Milky Way- to LMC- to SMC-type dust. Power-law fits to these curves over the wavelength range $0.1 \leq \lambda \leq 1 \mu\text{m}$ yield values of m between 1.1 and 1.5, with $m = 1.3$ representing a middle value (Fig. 9).

The ambient ISM of starburst galaxies cannot be idealized as a foreground screen if the dust within them is similar to that in the Milky Way, the LMC, or the SMC because the effective absorption curve would then take the form $\hat{\tau}_\lambda^{\text{ISM}} \propto \lambda^{-m}$ with $1.1 \lesssim m \lesssim 1.5$. As shown in §3, this would lead to a relation between L_{dust}/L_{1600} and β shallower than observed. We now examine the other two models of the ambient ISM specified in §2. Again, these should be regarded only as convenient approximations to more realistic distributions of dust. In the following, we adopt the same effective starburst age, t , lifetime of birth clouds, t_{BC} , and fraction of dust in the ionized gas, f , as in our standard model in §3 (eq. [30]).

We first consider the mixed slab model for the ambient ISM. In this case, $\hat{\tau}_\lambda^{\text{ISM}}$ is related to the optical depth through the slab in the direction normal to the surface,

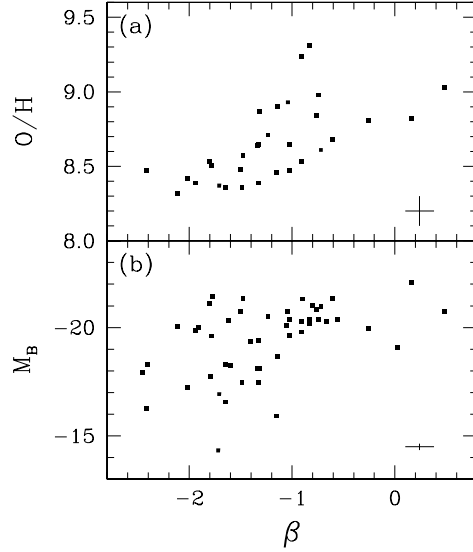


FIG. 8.— (a) Oxygen abundance plotted against ultraviolet spectral slope for galaxies in the Meurer et al. (1999) sample discussed in §3. The abundance measurements are from Calzetti et al. (1994). For reference, the solar abundance is $(\text{O}/\text{H})_{\odot} \approx 8.9$. (b) Absolute B magnitude plotted against ultraviolet spectral slope for the galaxies in the Meurer et al. (1999) sample. The adopted Hubble constant is $H_0 = 70 \text{ km s}^{-1} \text{ Mpc}^{-1}$. Typical measurement errors are indicated in each panel.

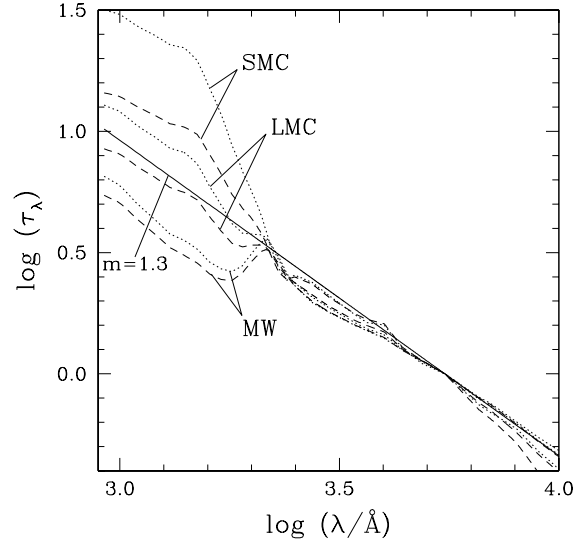


FIG. 9.— Optical depth of graphite-silicates dust plotted against wavelength. The dotted lines are the true absorption curves of the Milky Way, LMC, and SMC, while the dashed lines are the corresponding curves when isotropic scattering is included (eq. [19]). These are based on the Draine & Lee (1984) model but with the proportions of graphite and silicates adjusted so as to fit the observed mean extinction curves of the three galaxies (Pei 1992). The solid line is a power law of index $m = 1.3$. All curves are normalized to unity at 5500 \AA .

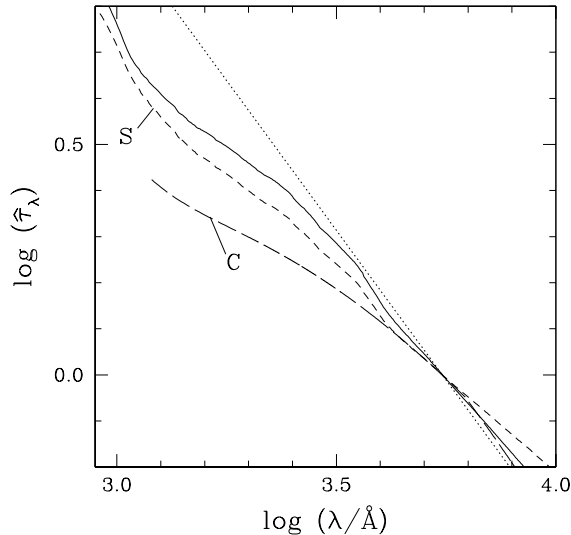


FIG. 10.— Effective absorption curve (as defined by eq. [4]) of a model with effective starburst age $t = 3 \times 10^8$ yr in which the ambient ISM is represented by a mixed slab (*solid line*). The optical depth of the dust is assumed to have the form $\tau_\lambda \propto \lambda^{-m}$ with $m = 1.3$ (*dotted line*). The short-dashed curve is the standard model of eq. (30), and the long-dashed curve is from Calzetti et al. (1994). All curves are normalized to unity at 5500 Å.

$\tau_\lambda^{\text{sl}} \propto \lambda^{-m}$, by equations (10) and (23). By analogy with our standard model in §3, we adopt $\hat{\tau}_V^{\text{BC}} = 1.0$ for the optical depth of the birth clouds and take $\tau_V^{\text{sl}} = 0.5$. Figure 10 shows the total effective absorption curve at $t = 3 \times 10^8$ yr with $m = 1.3$. A comparison with Figure 5 shows that this is very similar to the total effective absorption curve of the standard model with $n = 0.7$ in §3. To understand the origin of this result, we plotted $\hat{\tau}_\lambda^{\text{ISM}}$ as a function of τ_λ^{sl} and noticed that the simple formula $\hat{\tau}_\lambda^{\text{ISM}} \approx (\tau_\lambda^{\text{sl}})^{1/2}$ approximates $\hat{\tau}_\lambda^{\text{ISM}}$ with an accuracy of 5% or better over the whole range $1 \lesssim \tau_\lambda^{\text{sl}} \lesssim 10$ (at low optical depths, $\hat{\tau}_\lambda^{\text{ISM}}$ is closer to τ_λ^{sl}). This weak dependence of $\hat{\tau}_\lambda^{\text{ISM}}$ on τ_λ^{sl} arises from the fact that, for large τ_λ^{sl} , sources located at high optical depths from the surface of the slab contribute very little to the emergent light. In the ultraviolet, therefore, where τ_λ^{sl} is greater than unity, the wavelength dependence of $\hat{\tau}_\lambda^{\text{ISM}}$ is closer to $\lambda^{-m/2}$ than to λ^{-m} in the model of Figure 10. Hence, for reasonable assumptions about the optical properties of the dust, a mixed slab model for the ambient ISM can produce an effective absorption curve similar to that required by the observed relation between L_{dust}/L_{1600} and β .

Mixed slab models, however, cannot accommodate the full range of observations. In Figure 11, we show the analog of Figure 6 for models with $\hat{\tau}_V^{\text{BC}} = 2\tau_V^{\text{sl}}$ and $m = 1.3$. At low optical depths, i.e. for $\hat{\tau}_V^{\text{BC}} \lesssim 1$, the models reproduce well the observed relation between L_{dust}/L_{1600} and β , as noted above. At larger optical depths, however, the models deviate markedly from the observations. This upturn, which persists over the range $1.0 \leq m \leq 1.5$, is entirely a consequence of absorption in the ambient ISM because, for large optical depths of the birth clouds, i.e. for $\hat{\tau}_V^{\text{BC}} \gtrsim 1$, β and L_{dust}/L_{1600} are controlled by $\hat{\tau}_\lambda^{\text{ISM}}$ (Figs. 2c and 2d). The reason for this behavior can be

traced back to the fact that $\hat{\tau}_\lambda^{\text{ISM}}$ scales only as $(\tau_\lambda^{\text{sl}})^{1/2}$ for $\tau_\lambda^{\text{sl}} \gtrsim 1$. As τ_V^{sl} increases in Figure 11, $\hat{\tau}_\lambda^{\text{ISM}}$ approaches a power law of index $m/2$ over a range that expands toward progressively longer wavelengths (since $\tau_\lambda^{\text{sl}} \propto \tau_V^{\text{sl}} \lambda^{-m}$). Once the power-law shape extends over the entire ultraviolet wavelength range, increasing τ_V^{sl} no longer affects β but continues to alter L_{dust}/L_{1600} , $L_{\text{H}\alpha}/L_{\text{H}\beta}$, and $W_{\text{H}\alpha}$. This is an intrinsic limitation of the mixed slab model. For large τ_V^{sl} , β cannot reach the very large values observed because sources at high optical depths from the surface of the slab contribute very little to the emergent ultraviolet radiation.

We now consider the discrete cloud model for the ambient ISM. In this case, $\hat{\tau}_\lambda^{\text{ISM}}$ is related to the optical depth per cloud, $\tau_\lambda^c \propto \lambda^{-m}$, and the mean number of clouds along a line of sight, \bar{n} , by the expression $\hat{\tau}_\lambda^{\text{ISM}} = \bar{n} [1 - \exp(-\tau_\lambda^c)]$ (eqs. [10] and [25]). Thus, \bar{n} does not affect the wavelength dependence of $\hat{\tau}_\lambda^{\text{ISM}}$. To illustrate the effective absorption curves of the discrete cloud models, we fix $\hat{\tau}_V^{\text{BC}} = 1.0$ and experiment with different optical depths of the clouds, $\tau_V^c = 0.1, 0.3$, and 0.5 . By analogy with our standard model in §3, we adjust \bar{n} so that the mean optical depth along a line of sight is $\bar{n}\tau_V^c = 0.5$ in each case. Figure 12 shows the total effective absorption curves at $t = 3 \times 10^8$ yr for these models with $m = 1.3$. The models exhibit the characteristic signatures of the absorption in the birth clouds (Fig. 5). As τ_V^c increases, $\hat{\tau}_\lambda$ becomes greyer because the wavelength below which the clouds absorb all incident radiation, i.e. where $\hat{\tau}_\lambda^{\text{ISM}} \approx \bar{n}$, becomes progressively larger. Figure 12 indicates that the model with $\tau_V^c = 0.3$ has the ultraviolet slope closest to that of the standard model in §3. For reasonable assumptions about the optical properties of the dust, therefore, discrete cloud models also lead to effective absorption curves similar to that required by the observed relation between L_{dust}/L_{1600} and β .

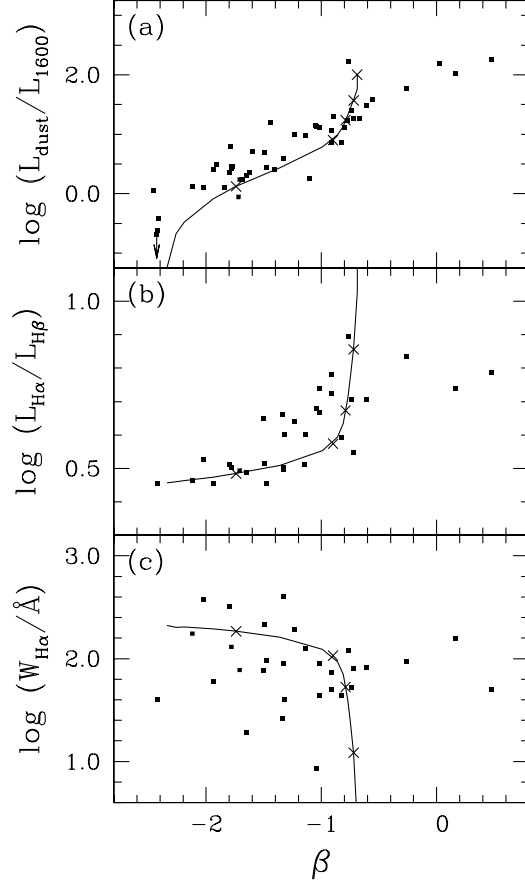


FIG. 11.— Sequence of models in which the ambient ISM is represented by a mixed slab with different dust content and $\hat{\tau}_V^{\text{BC}} = 2\tau_V^{\text{sl}}$. The optical depth of the dust is assumed to have the form $\tau_\lambda \propto \lambda^{-m}$ with $m = 1.3$. Crosses mark the models with $\hat{\tau}_V^{\text{BC}} = 0.1, 0.5, 1.0, 2.0,$ and 5.0 (in order of increasing β) to indicate the scale. The data points in (a), (b), and (c) are the same as in Figs. 2, 3, and 4, respectively.

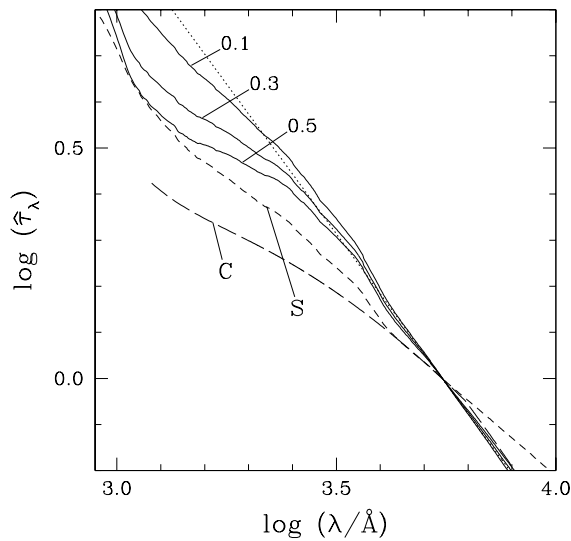


FIG. 12.— Effective absorption curves (as defined by eq. [4]) of models with effective starburst age $t = 3 \times 10^8$ yr in which the ambient ISM is represented by a Poisson distribution of clouds. The optical depth of the dust is assumed to have the form $\tau_\lambda \propto \lambda^{-m}$ with $m = 1.3$ (dotted line). The models are shown for different cloud optical depths, $\tau_V^c = 0.1, 0.3,$ and 0.5 (as indicated). The short-dashed curve is the standard model of eq. (30), and the long-dashed curve is from Calzetti et al. (1994). All curves are normalized to unity at 5500 \AA .

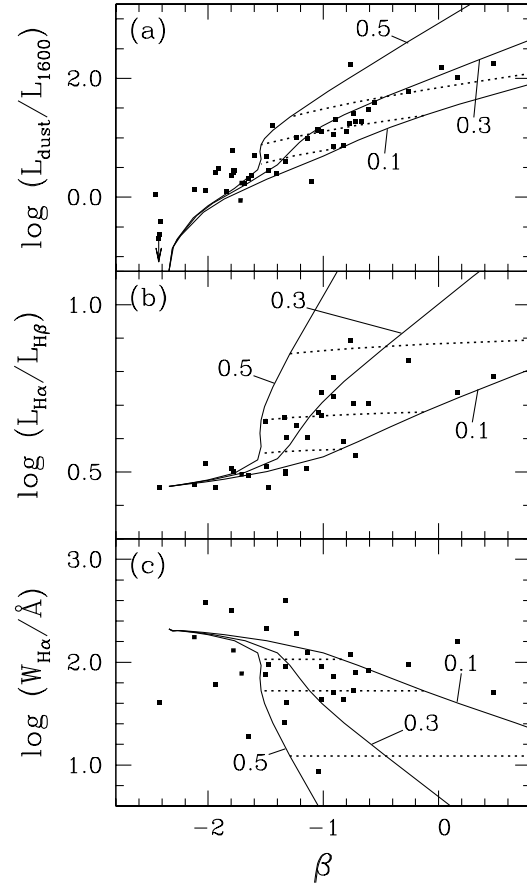


FIG. 13.— Sequences of models in which the ambient ISM is represented by a Poisson distribution of clouds with different dust content and $\hat{\tau}_V^{\text{BC}} = 2\bar{n}\tau_V^c$. The optical depth of the dust is assumed to have the form $\tau_\lambda \propto \lambda^{-m}$ with $m = 1.3$. The models are shown for different cloud optical depths, $\tau_V^c = 0.1, 0.3$, and 0.5 (as indicated). Dotted lines join models with $\hat{\tau}_V^{\text{BC}} = 0.5, 1.0$, and 2.0 (in order of increasing β) to indicate the scale. The data points in (a), (b), and (c) are the same as in Figs. 2, 3, and 4, respectively.

The advantage of discrete cloud models over mixed slab models is that they can account for the full range of observations. In Figure 13, we show the analog of Figure 6 for models with $\hat{\tau}_V^{\text{BC}} = 2\bar{n}\tau_V^c$, \bar{n} a continuous variable, $\tau_V^c = 0.1, 0.3$, and 0.5 , and $m = 1.3$. The models with $\tau_V^c = 0.3$ agree with all the observations. In particular, they match remarkably well the relations between L_{dust}/L_{1600} , $L_{\text{H}\alpha}/L_{\text{H}\beta}$, and β over the entire range observed. Models with $\tau_V^c = 0.5$ and 0.1 lie above and below those with $\tau_V^c = 0.3$, as expected from the different effective absorption curves in Figure 12. The mean number of clouds in the models with $\tau_V^c = 0.3$ ranges from $\bar{n} = 0$ at one end of the relations (with $\beta = -2.3$) to $\bar{n} \approx 5$ at the other end (with $\beta \approx +0.2$). These values of \bar{n} are small enough that the distribution of dust can be regarded as patchy over most of the range. We also find that the relations between L_{dust}/L_{1600} , $L_{\text{H}\alpha}/L_{\text{H}\beta}$, and β are very stable to m over the range $1.0 \leq m \leq 1.5$ for $\tau_V^c = 0.3$, but curiously less stable for $\tau_V^c = 0.1$ and 0.5 . The above values of τ_V^c would be somewhat smaller if we had adopted an optical depth τ_λ with a strong feature near 2175 \AA .

Our results demonstrate that, for reasonable assumptions about the wavelength dependence of the dust optical depth τ_λ , discrete cloud models can account for all the observed integrated spectral properties of nearby starburst galaxies. Poisson distributions of clouds have traditionally been used to interpret variations in the observed reddening of stars at the same distance within the Milky Way. These observations can be well represented by a model with two types of clouds, one with $A_V^c \approx 0.2$ and another, less abundant one with $A_V^c \approx 0.9$ (Spitzer 1978). This is similar to our model, which has a population of optically thin clouds in the ambient ISM and a population of optically thick birth clouds. It is worth emphasizing that in any model with discrete clouds, the optical depth has a large variance along different lines of sight within a given galaxy, depending on the number of clouds encountered. In particular, some lines of sight can be quite opaque, even for $\tau_V^c = 0.3$ and $\bar{n} \sim 1$. For starburst galaxies with the largest values of L_{dust}/L_{1600} , $\bar{n} \approx 5$ is indicated, and most lines of sight are opaque. Thus, there is no contradiction between the relatively small values of τ_V^c found here and the very dusty appearance of some starburst galaxies.

5. CONCLUSIONS

We have developed a simple model to compute the effects of dust on the integrated spectral properties of galaxies, based on an idealized prescription of the main features of the ISM. Our model includes the ionization of HII regions in the interiors of the dense clouds in which stars form. Emission lines from HII regions and the non-ionizing continuum from young stars are attenuated in the same way by dust in the outer HI envelopes of the birth clouds and the ambient ISM. However, since the model also includes the finite lifetimes of the birth clouds, the non-ionizing continuum radiation from stars that live longer than the birth clouds is attenuated only by the ambient ISM. We show that this can fully resolve the apparent discrepancy between the attenuation of line and continuum photons in starburst galaxies. This enables us, in turn, to interpret in a consistent way all the observations of a homogeneous sample of nearby ultraviolet-selected starburst

galaxies, including the ratio of far-infrared to ultraviolet luminosities (L_{dust}/L_{1600}), the ratio of H α to H β luminosities ($L_{\text{H}\alpha}/L_{\text{H}\beta}$), the H α equivalent width ($W_{\text{H}\alpha}$), and the ultraviolet spectral slope (β).

The different parameters in our model, including the effective age of the starburst, the lifetime and effective optical depth of the stellar birth clouds, the effective optical depth in the ambient ISM, and the fraction of dust in the ionized gas, each have a specific influence on the integrated spectral properties L_{dust}/L_{1600} , $L_{\text{H}\alpha}/L_{\text{H}\beta}$, $W_{\text{H}\alpha}$, and β . This provides new insights into the origin of the mean relations defined by the data and the scatter about these relations. In particular, the relation between the ratio of far-infrared to ultraviolet luminosities and the ultraviolet spectral slope in starburst galaxies reflects the wavelength dependence of the effective absorption in the ambient ISM. We find that a power law of the form $\hat{\tau}_\lambda^{\text{ISM}} \propto \lambda^{-0.7}$ accounts remarkably well for all the observations. The relation between L_{dust}/L_{1600} and β can then be interpreted as a sequence in the overall dust content of the galaxies. Interestingly, this relation is accompanied by much weaker trends of the oxygen abundance and the optical luminosity with the ultraviolet spectral slope. The fact that our model reproduces the observed spectral properties of nearby starburst galaxies relatively easily leads us to suspect that, with suitable adjustment of the parameters, it could also reproduce those of more quiescent (but still star-forming) galaxies.

The effective absorption curve required by the observations is much greyer than would be produced by a foreground screen of dust like that in the Milky Way, the LMC, or the SMC. We have explored whether this could be accounted for by a much steeper wavelength dependence of the optical depth, i.e. $\tau_\lambda \propto \lambda^{-m}$ with $1.0 \lesssim m \lesssim 1.5$, combined with a more realistic spatial distribution of the dust. We find that a mixed slab model for the ambient ISM can produce the required effective absorption curve for low dust content but cannot explain the observations of starburst galaxies with very reddened ultraviolet spectra. In contrast, we show that a random distribution of discrete clouds provides a consistent interpretation of all the observed integrated spectral properties of starburst galaxies. While these results were anticipated in some previous studies, we have shown here for the first time how to reconcile them with the large H α /H β ratios and other observations. We also find that the optical depths of the clouds favored by our analysis are similar to those inferred from the statistics of stellar reddening in the Milky Way.

The model we have developed for computing the absorption of starlight by dust in galaxies can be combined easily, by design, with any population synthesis model. The observed mean relations for starburst galaxies can also be reproduced by the following simple recipe: use an effective absorption curve proportional to $\lambda^{-0.7}$ to attenuate the line and continuum radiation from each stellar generation, and lower the normalization of the curve typically by a factor of 3 after 10^7 yr to account for the dispersal of the birth clouds. This recipe accounts at least as well as the one by Calzetti et al. (1994, and as modified by Calzetti 1997, 1999) for the effects of dust on the non-ionizing continuum radiation. In addition, it fully resolves the apparent discrepancy between the attenuation of line and contin-

uum photons in starburst galaxies. We believe, therefore, that our model and the recipe derived from it provide simple yet versatile tools to interpret the integrated spectral properties of starburst and possibly other types of galaxies. In future work, we plan to apply them to the growing body of observations of high-redshift galaxies.

We thank P. Boissé, A. Ferrara, and N. Panagia for valuable discussions. S.C. appreciates the hospitality of the STScI, and S.M.F. that of the IAP, during the course of several visits. This research was supported in part by the National Science Foundation through grant no. PHY94-07194 to the Institute for Theoretical Physics.

REFERENCES

- Bianchi, S., Ferrara, A., & Giovanardi, C. 1996, *ApJ*, 465, 127
 Blitz, L., & Shu, F. H. 1980, *ApJ*, 238, 148
 Bottorff, M., LaMothe, J., Momjian, E., Verner, E., Vinković, & Ferland, G. 1998, *PASP*, 110, 1040
 Bruzual, A. G., & Charlot, S. 1993, *ApJ*, 405, 538
 Bruzual, A. G., Magris, G., & Calvet, N. 1988, *ApJ*, 333, 673
 Calzetti, D. 1997, *AJ*, 113, 162
 ———. 1999, private communication
 Calzetti, D., Bohlin, R. C., Gordon, K. D., Witt, A. N., & Bianchi, L. 1995, *ApJ*, 446, L97
 Calzetti, D., Kinney, A. L., & Storchi-Bergmann, T. 1994, *ApJ*, 429, 582
 ———. 1996, *ApJ*, 458, 132
 Caplan, J., & Deharveng, L. 1986, *A&A*, 155, 297
 Di Bartolomeo, A., Barbaro, G., & Perinotto, M. 1995, *MNRAS*, 277, 1279
 Disney, M., Davies, J., & Phillipps, S. 1989, *MNRAS*, 239, 939
 Draine, B. T., & Lee, H. M. 1984, *ApJ*, 285, 89
 Fanelli, M. N., O'Connell, R. W., & Thuan, T. X. 1988, *ApJ*, 334, 665
 Ferland, G. J. 1996, in *Hazy, a Brief Introduction to Cloudy*, Univ. of Kentucky Dept. of Physics & Astronomy Int. Rep.
 Gordon, K. D., Calzetti, D., & Witt, A. N. 1997, *ApJ*, 487, 625
 Helou, G., Khan, I. R., Malek, L., & Boehmer, L. 1988, *ApJS*, 68, 151
 Hummer, D., & Storey, P. 1992, *MNRAS*, 254, 277
 Humphreys, R. M. 1978, *ApJS*, 38, 309
 Kim, S.-H., Martin, P. G., & Hendry, P. D. 1994, *ApJ*, 422, 164
 Kinney, A. L., Bohlin, R. C., Calzetti, D., Panagia, N., & Wyse, R. F. G. 1993, *ApJS*, 86, 5
 McQuade, K., Calzetti, D., & Kinney, A. L. 1995, *ApJS*, 97, 331
 Meurer, G. R., Heckman, T. M., & Calzetti, D. 1999, *ApJ*, 521, 64
 Meurer, G. R., Heckman, T. M., Leitherer, C., Kinney, A., Robert, C., & Garnett, D. R. 1995, *AJ*, 110, 2665
 Mezger, P. G., & Smith, L. F. 1977, in *IAU Symp. 75, Star Formation*, ed. T. de Jong & A. Maeder (Dordrecht: Reidel), 133
 Natta, A., & Panagia, N. 1984, *ApJ*, 287, 228
 Oey, M. S., & Kennicutt, R. C. 1997, *MNRAS*, 291, 827
 Osterbrock, D. E. 1989, *Astrophysics of Gaseous Nebulae and Active Galactic Nuclei* (Mill Valley: University Science Books)
 Pei, Y. C. 1992, *ApJ*, 395, 130
 Petrosian, V., Silk, J., & Field, G. B. 1972, *ApJ*, 117, L69
 Puxley, P. J., & Brand, P. W. J. L. 1994, *MNRAS*, 266, 431
 Rybicki, G. B., & Lightman, A. P. 1979, *Radiative Processes in Astrophysics* (New York: Wiley), 36
 Silva, L., Granato, G. L., Bressan, A., & Danese, L. 1998, *ApJ*, 509, 103
 Spitzer, L. 1978, *Physical Processes in the Interstellar Medium* (New York: Wiley), 154
 Storchi-Bergmann, T., Kinney, A. L., & Challis, P. 1995, *ApJS*, 98, 103
 Witt, A. N., & Gordon, K. D. 1996, *ApJ*, 463, 681
 Witt, A. N., Thronson, H. A., & Capuano, J. M. 1992, *ApJ*, 393, 611